Counting primary loops in polymer gels

Counting primary loops in polymer gels

Huaxing Zhou[a], Jiyeon Woo[a], Alexandra M. Cok[a], Muzhou Wang[b], Bradley D. Olsen[b], and Jeremiah A. Johnson[a,1]

Departments of [a]Chemistry and [b]Chemical Engineering, Massachusetts Institute of Technology, Cambridge, MA 02139

Edited by David A. Weitz, Harvard University, Cambridge, MA, and approved October 9, 2012 (received for review July 31, 2012)

Much of our fundamental knowledge related to polymer networks is built on an assumption of ideal end-linked network structure. Real networks invariably possess topological imperfections that negatively affect mechanical properties; modifications of classical network theories have been developed to account for these defects. Despite decades of effort, there are no known experimental protocols for precise quantification of even the simplest topological network imperfections: primary loops. Here we present a simple conceptual framework that enables primary loop quantification in polymeric materials. We apply this framework to measure the fraction of primary loop junctions in trifunctional PEG-based hydrogels. We anticipate that the concepts described here will open new avenues of theoretical and experimental research related to polymer network structure.

responsive materials | topology | network disassembly spectrometry | tetrazine

The properties of all known polymer networks, from commodity materials like nylon, rubber, and plastics, to biological tissues such as the extracellular matrix (ECM) and cartilage, are defined by the network's chemical composition and structural topology (1–3). Much of our fundamental knowledge related to polymer materials, e.g., theories of elasticity and gelation, was built more than half a century ago upon an assumption of ideal end-linked network structure (Fig. 1*A*) (2, 4–7). Real networks invariably possess imperfections such as first-order elastically inactive dangling chains and primary loops (Fig. 1*B*), and higher-order elastic loop structures and chain entanglements; modifications of classical network theories have been developed to account for these defects (8–11).

First-order network imperfections (Fig. 1*B*) have the most direct negative impact on the mechanical properties of materials. Dangling chains can be minimized if efficient end-linking reactions are used between functional groups present at 1:1 ratio. In contrast, kinetic constraints demand that primary loops exist regardless of functional group conversion (12). Unlike dangling chains, which can be readily quantified via titration or spectroscopy, there are no known methods for quantification of primary loops. Their prevalence is estimated from pregel measurements or variations between the properties of a given material and theoretical model networks (2, 4, 7–9, 12–17). These molecular-level mechanical imperfections could critically impact modern applications of polymer networks and gels (18–28), especially those built on an end-linked network architecture (29–33).

Here we present a simple conceptual framework called network disassembly spectrometry (NDS) that enables facile, simultaneous quantification of the fraction of primary loops and the numbers and structures of dangling chains in end-linked materials via site-selective network disassembly. We apply this framework to degradable PEG hydrogels, which are similar to materials frequently used in tissue engineering applications (29, 32).

NDS Concepts

Site-specific polymer cleavage is one of nature's ubiquitous strategies for modulating biopolymer properties and controlling cellular interactions with the ECM (34). The same concept is commonly used to study the structures of macromolecules and control the mechanical properties of synthetic polymer networks (29, 32, 35–39). Consider a general end-linked network comprised of R-A_2 and R′-B_f monomers where f represents the network branch functionality. The fraction of primary loops, n_λ, in this network can be measured if R-A_2 and R′-B_f satisfy two constraints: all A_2 and B_f groups must be equally reactive, or their relative reactivities must be known, and one of the network precursors must contain an appropriately placed cleavable group or groups such that cleavage yields distinct, identifiable products.

There are many possible ways to meet the latter criterion. For simplicity, we demonstrate the NDS concept by using an R-A_2 monomer that cleaves along the R backbone to generate products with distinct masses: "short" (S) and "long" (L; Fig. 2*A*). Such a species is referred to as an "asymmetrically-degradable" monomer (ADM). Fig. 2*B* shows a schematic network that would result from coupling this R-A_2 ADM and a hypothetical R′-B_3 monomer. The possible network junctions can be identified by the orientations of S and L chains. In the case of 100% functional group conversion, there are four possible junctions: three S chains (i.e., SSS junction), two S and one L chain (i.e., SSL junction), one S and two L chains (i.e., SLL junction), and three L chains (i.e., LLL junctions). Because of the asymmetric nature of the ADM, primary loops cannot exist at SSS or LLL junctions. Therefore, as n_λ increases, the fraction of SSS and LLL junctions must decrease.

Network disassembly via cleavage of the R-A_2 ADM yields soluble products whose masses are unique for each junction orientation (Fig. 2*C*). This collection of disassembly products constitutes a "network disassembly spectrum" that contains the dangling chain content and the primary loop fraction. The ratio of LLL or SSS to SLL or SSL quantifies primary loops in terms of a "loop ratio," λ_3, where the subscript "3" refers to the network functionality f. A simple statistical analysis reveals that λ_3 varies from one third to zero as n_λ increases from zero (ideal network) to one (only primary loops) according to Eq. **1** in Fig. 2*D*.

The same concept outlined here for trifunctional networks applies to networks of higher branch functionality (i.e., $f > 3$), to networks with polydisperse branch functionality, and to linear step-growth polymerizations (i.e., $f = 2$). Namely, the ratio of the largest disassembly product to the next largest disassembly product (or the smallest to the next smallest) for each f will always vary directly with the fraction of primary loops within the material. The general loop ratio, λ_f, as a function of f, is given in *SI Appendix*, Eq. S1.

Gel Precursor Design and Synthesis

To demonstrate NDS, hydrogels were prepared via Diels–Alder end-linking of norbornene-telechelic PEG oligomer M (R-A_2 ADM) and tris-tetrazine T (R′-B_3; Fig. 3*A*; *SI Appendix* describes synthetic procedures) (40–42). M possesses a single ester group, which when cleaved yields S and L products. The norbornene and tetrazine functional groups from M and T, respectively, should react randomly to avoid a biased distribution of network junction structures. Pseudo–first-order kinetic plots for the reaction of M with excess of

Author contributions: B.D.O. and J.A.J. designed research; H.Z., J.W., A.M.C., M.W., B.D.O., and J.A.J. performed research; M.W., B.D.O., and J.A.J. contributed new reagents/analytic tools; H.Z., M.W., B.D.O., and J.A.J. analyzed data; and J.A.J. wrote the paper.

The authors declare no conflict of interest.

This article is a PNAS Direct Submission.

[1]To whom correspondence should be addressed. E-mail: jaj2109@mit.edu.

This article contains supporting information online at www.pnas.org/lookup/suppl/doi:10.1073/pnas.1213169109/-/DCSupplemental.

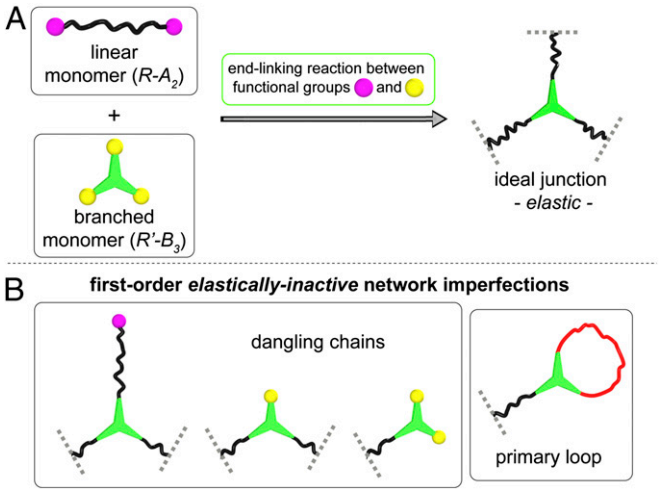

Fig. 1. End-linked networks. (*A*) Schematic depiction of a general end-linked polymer network obtained from coupling a linear, bifunctional monomer (R-A_2) and a branched, trifunctional monomer (R′-B_3). (*B*) Two-dimensional projections of common first-order network imperfections.

a monotetrazine derivative (*SI Appendix*, Fig. S1) were linear through complete norbornene conversion. Similarly, pseudo–first-order kinetic plots for reaction of T with a monofunctional norbornene-tetraethylene glycol (*SI Appendix*, Fig. S2) were linear through complete tetrazine conversion. These data strongly suggest that reactions of functional groups within M and T are random.

End-linking reactions between M and T were prepared with equimolar concentrations of functional groups (1:1 norbornene: tetrazine) in DMSO solvent at room temperature. The initial concentration of M, $[M]_0$, was varied from 2 mM to 80 mM (examples shown in Fig. 3*A*). Immediately after mixing M and T, the reaction solutions possessed a deep red color as a result of tetrazine absorbance (Fig. 3*A*). As tetrazine groups were consumed, the reactions turned from red to orange and then to light yellow; the reactions were allowed to proceed until no further color change was observed (*SI Appendix*, Fig. S3).

When $[M]_0$ was < 60 mM, soluble network polymers were obtained. This observation suggested that at least 29.3% of the functional groups from M and T were consumed in cyclization reactions (2). These materials were characterized by liquid chromatography(LC)/MS and gel permeation chromatography (*SI Appendix*, Fig. S4). Low mass primary loop products (e.g., dumbbell polymers) were directly observed in these soluble materials prior to disassembly; quantification of the ratio of primary loop junctions to ideal network junctions was impossible as a result of the intractable number of high mass products that must also possess primary loops.

Reactions performed at $[M]_0$ of ≥ 60 mM formed gels that swelled extensively without dissolution. Fig. 3*B* shows the chemical structure of an SSS network junction. There are three possible dipyridyl-dihydropyridazine (DPDHP) isomers at each reaction site. These junctions were converted to a single aromatic dipyridyl-pyridazine isomer via treatment with 2,3-dichloro-5,6-dicyano-*p*-benzoquinone (DDQ; Fig. 3*C* and *SI Appendix*, Fig. S4). This oxidation has no impact on the orientations of S and L chains; it was performed to enable facile quantification of the network disassembly products via absorbance. The resulting oxidized networks, referred to as gel(O), were studied via NDS as outlined below.

Network Disassembly and Measurement of Loop Ratio

To measure the ratios of SSS, SSL, SLL, and LLL junctions (Fig. 4*A*), gel(O) networks were hydrolyzed under basic conditions (Fig. 3*C*). Samples of an M+T end-linking reaction were taken at various time points, oxidized with DDQ, hydrolyzed, and subjected to LC/MS. The corresponding network disassembly spectra show the evolution of junction structures before and after the gel point (Fig. 4*B*; gelation occurs at ~30 min). These kinetic NDS studies provide snapshots of junction structure evolution during a gelation reaction as it proceeds from mostly dangling chain species to trifunctional junctions.

Fig. 4*C* shows a typical network disassembly spectrum after 100% conversion and removal of sol fractions. Four products are observed in the absorbance trace (A_{350}; Fig. 4*C*; green dashed line). Six species were observed in the mass trace; they correspond to SSS, SSL, SLL, and LLL, along with S and L molecular ions from dangling chains (extracted ion count traces; Fig. 4*C*). Mass spectra for each of the trifunctional products are shown in *SI Appendix*, Fig. S5. The observation of three to four multiply charged ions for each

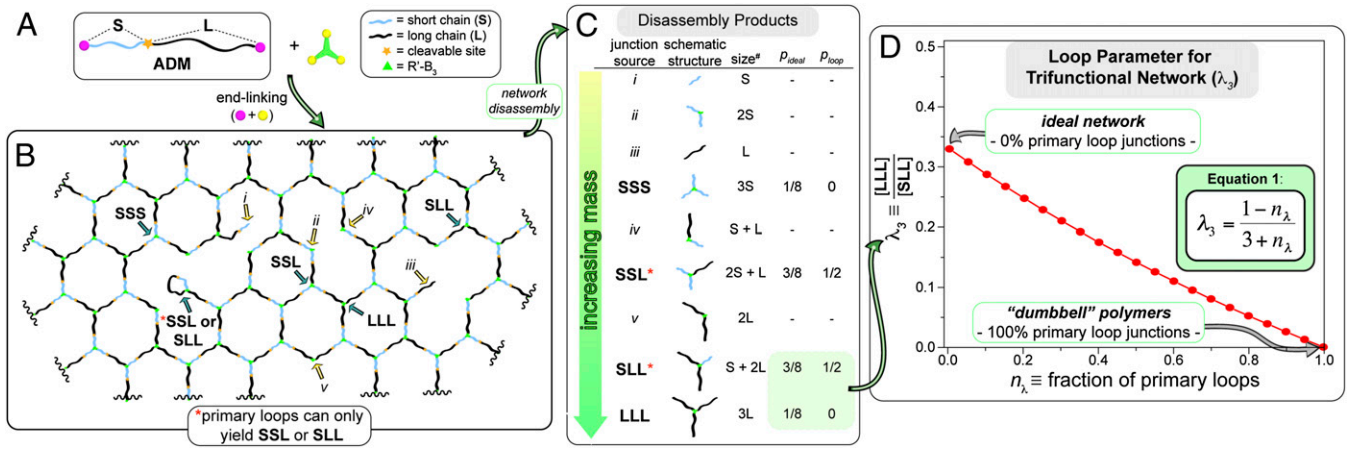

Fig. 2. NDS. (*A*) Schematic depiction of an R-A_2 ADM. Placement of a degradable group (orange star) at a noncentral position along the R-A_2 backbone leads to an S chain (blue) and an L chain (black) after cleavage. (*B*) End-linking of R-A_2 and R′-B_3 yields a network in which each network junction is unique in terms of the orientation of S and L chains. Primary loops (asterisks) cannot reside at SSS or LLL junctions. (*C*) Disassembly of the network yields products whose masses depend on the junction source of that product. (#Product size, or relative mass, does not include the mass of R′-B_3, which is assumed to be constant.) The probabilities for formation of each trifunctional product at ideal or loop junctions are listed as p_{ideal} and p_{loop}, respectively. The number of primary loops is captured in the ratio [LLL]:[SLL] or λ_3. (*D*) Plot of the loop ratio, λ_3, vs. fraction of loop junctions, n_λ, for a trifunctional network; λ_3 varies with n_λ according to Eq. **1**. Fully looped "dumbbell" polymers have loop-linear-loop architectures.

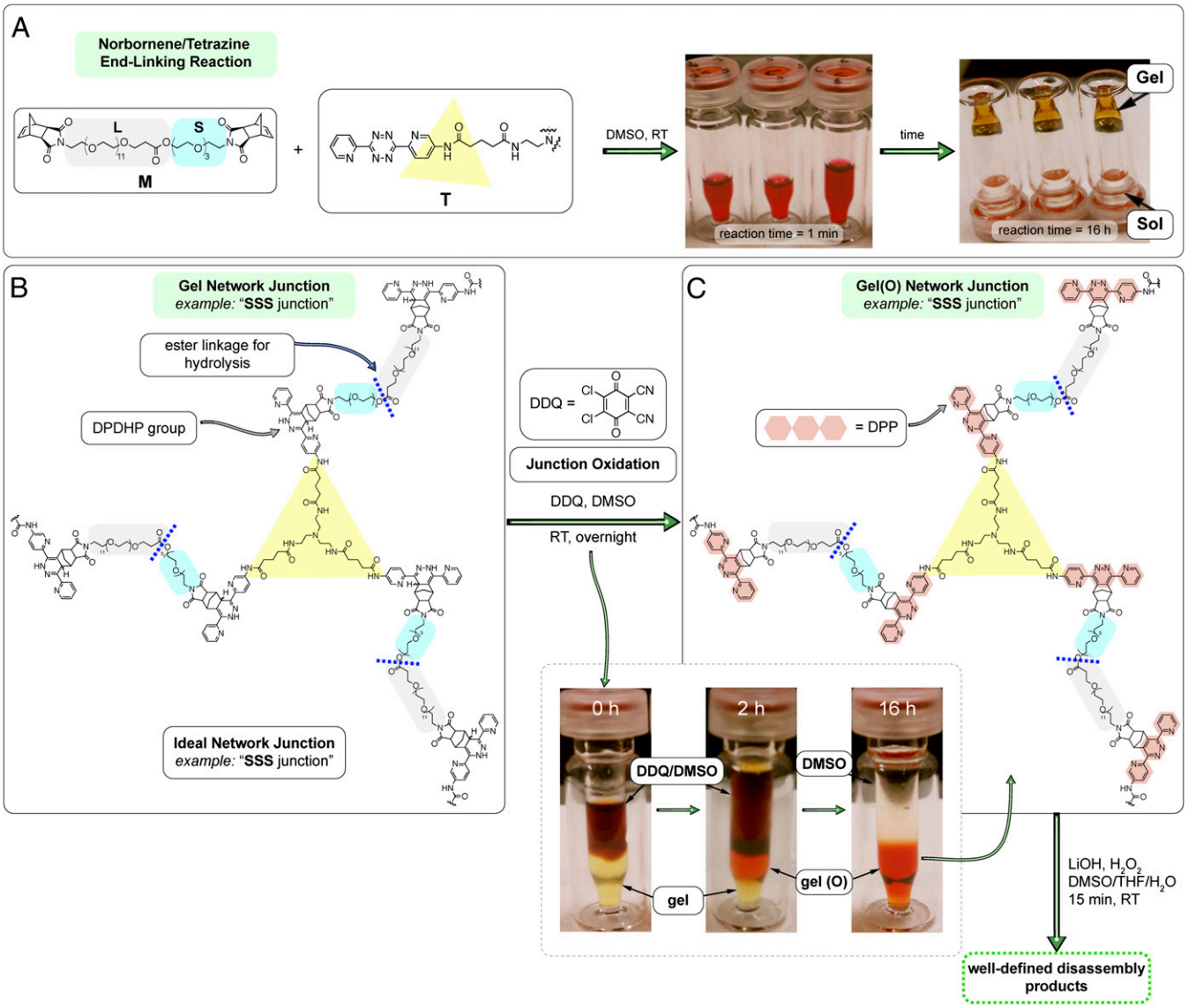

Fig. 3. Synthesis of PEG gel(O). (*A*) Structures of ADM M and tritetrazine T used in this study. Conversion of the dark red dipyridyl-tetrazine groups to light yellow DPDHP allowed facile monitoring of the end-linking conversion with time. (*B*) After gel formation, junctions are connected by DPDHP linkages. The SSS junction is shown. (*C*) Treatment of gels with DDQ led to oxidation of the DPDHP linkages to aromatic dipyridyl-pyridazine (DPP) groups [gel(O) networks]. Gel(O) materials were disassembled via ester hydrolysis in the presence of $LiOH/H_2O_2$.

product allows unambiguous assignment to SSS, SSL, SLL, and LLL. We did not observe any products from unreacted tetrazine junctions. The observed S and L products arise from a very small fraction of norbornene dangling chain ends within the parent network, which are the result of a slight norbornene/tetrazine stoichiometry imbalance.

Loop Ratios and Loop Fractions

Increased M dilution during end-linking should yield a greater number of primary loops. Fig. 5*A* shows network disassembly spectra obtained for varied $[M]_0$. The two peaks correspond to SLL and LLL; they are normalized to the height of the SLL peak. The LLL peak is clearly diminished with increased dilution. The most dilute samples (2 mM) yielded no LLL in the A_{350} chromatogram and only a trace amount in the A_{254}, which indicates that loop structures are formed almost exclusively at this concentration. LC/MS of this sample confirms that it is composed primarily of cyclic dumbbell polymer structures (*SI Appendix*, Fig. S4*E*).

The UV absorbance peaks for SLL and LLL from four or five samples of each $[M]_0$ were integrated to yield λ_3 as a function of $[M]_0$ (Fig. 5*B* and *SI Appendix*, Table S1). For $[M]_0$ values that yielded gels, three different λ_3 values were collected: one "average" ($\lambda_{3,ave}$) obtained without separation of sol and gel, a gel value ($\lambda_{3,gel}$) obtained after extensive extraction of the sol, and a sol value ($\lambda_{3,sol}$) derived from the extracted soluble material. As shown in Fig. 5*B*, the $\lambda_{3,gel}$ values approach the ideal network value of one third as $[M]_0$ increases, whereas $\lambda_{3,sol}$ values are consistently ~0.18.

Eq. **1** (Fig. 2*D*) was used to convert the measured loop ratios to n_λ values. Fig. 5*C* shows a plot of n_λ vs. $[M]_0$. Regions of the plots from Fig. 5 *B* and *C* are shaded to reflect the nature of the network products: orange and blue regions correspond to soluble networks and sol fractions, respectively, whereas the green regions correspond to gels. The fraction of unreacted functionality at the gel point in ideal trifunctional networks as defined by Flory–Stockmayer theory is 0.293 (2, 4). This value is shown in Fig. 5*C* as a green dotted line. All the soluble materials have n_λ of ≥ 0.30, whereas gel samples have average n_λ values less than 0.30. The

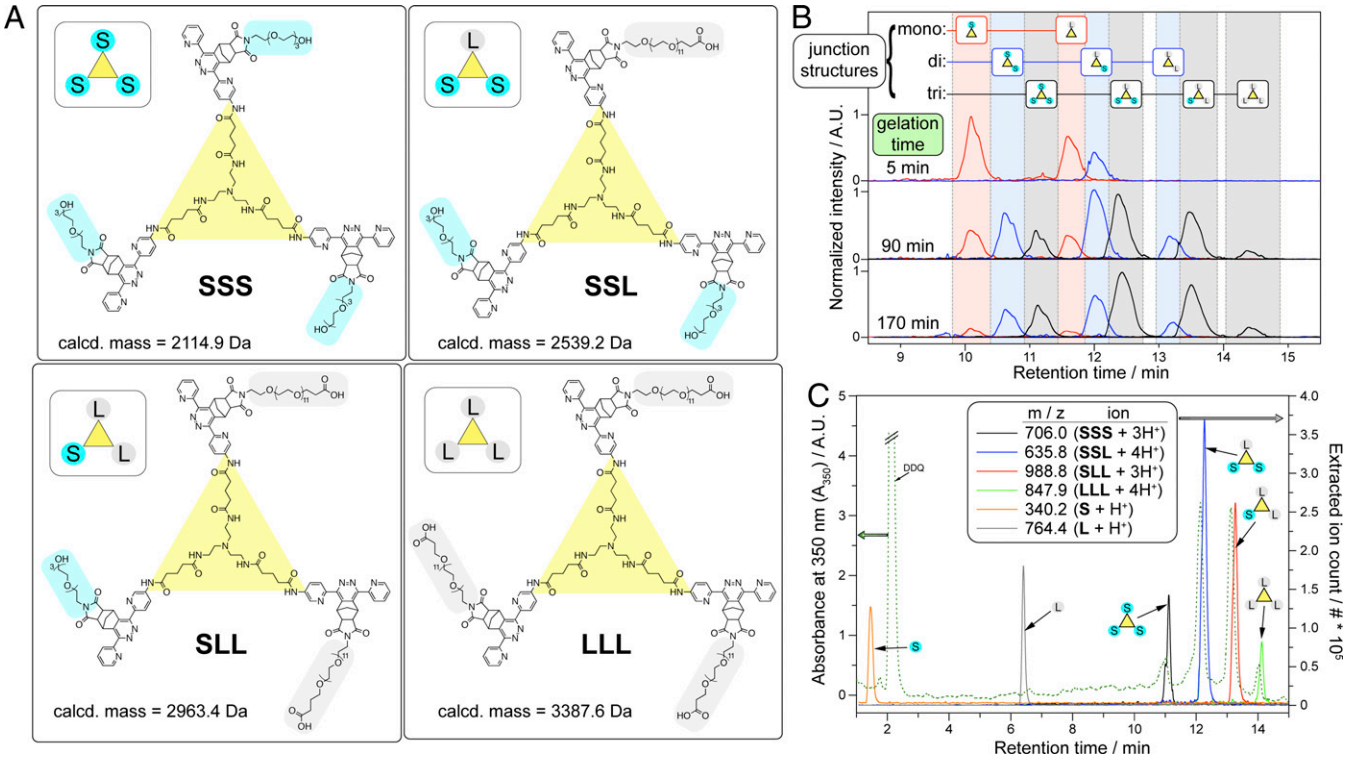

Fig. 4. Network disassembly spectra for gel(O). (*A*) Structures and calculated masses of the SSS, SSL, SLL, and LLL products expected for gel(O) networks. (*B*) Network disassembly spectra as a function of end-linking time. Each of the possible products from Fig. 2*C* are observed. With time, the fraction of trifunctional products (black traces) begins to dominate. (*C*) Network disassembly spectrum after 100% tetrazine conversion. Four peaks were observed in the absorbance trace (green dotted line; A_{350}). Extracted ion traces are shown for observed disassembly products. The key SSS, SSL, SLL, and LLL products elute in order of their masses; the ratio [LLL]:[SLL] can be readily obtained via integration of the last two A_{350} peaks. The S and L peaks result from dangling chains.

results provide convincing evidence that primary loop formation defines the outcome of the gelation reaction; higher-order loops and/or chain entanglements, which cannot be measured, are negligible. The gels alone, after sol extraction, all have loop fractions less than 0.20. Surprisingly, even the gels prepared at the highest concentration experimentally accessible (80 mM) possessed 9% primary loop junctions. These data highlight the pervasive nature of elastically inactive loops in polymeric materials.

If the principle of equal reactivity (2) holds for a given set of network formation conditions, the rates of loop formation and ideal junction formation should vary equally as a function of temperature; λ_f should remain constant. The values of λ_3 for $[M]_0$ of 30-mM and 60-mM networks prepared at 70 °C were 0.16 ± 0.01 and 0.26 ± 0.01, respectively. These values are identical to those obtained for the same $[M]_0$ at room temperature, which provides direct support for the principle of equal reactivity in this system.

Comparison of Loop Fractions vs. Theoretical Predictions

The loop fraction values shown in Fig. 5*C* were compared with rate theory (10, 43) and Monte Carlo (MC) simulation (44) methods developed by Stepto. For both theories, M was modeled as a linear, bivalent, telechelic Gaussian chain R-A_2 with a mean-square end-to-end distance of $\langle r^2\rangle_0$, and T was modeled as a trivalent point particle R′-B_3. In all cases, A and B groups are present in equimolar amounts and reactions are carried to 100% conversion.

Fig. 5*C* shows the calculated loop fractions vs. concentration. The theories predict similar dependences of primary loop fraction on concentration that are in excellent agreement with the experimental $\lambda_{3,ave}$ values. Both theories contain a single variable parameter of $\langle r^2\rangle_0$, which can be estimated by using published values (45) of PEG chain dimensions: for M of 1,085 Da, $\langle r^2\rangle_0$ is 8.7nm^2. A least-squares fit of the MC simulation results to the experimental primary loop fractions yielded $\langle r^2\rangle_0$ of 9.2 nm^2, whereas a least-squares fit of the rate theory to the experimental primary loop fractions results in a value of 9.0 nm^2. Both of these fits are in excellent agreement with the theoretically predicted size of the polymer chain, suggesting that the models provide satisfactory predictive capacity for this data set with no adjustable parameters. The theories do not, however, readily generate loop fraction values for the separate sol ($\lambda_{3,sol}$) and gel ($\lambda_{3,gel}$) components, which are the relevant values for applications of gels. To obtain these values, extensive further theoretical analysis would be required.

Junction connectivities obtained from MC simulation were visualized by using molecular dynamics. A simulated gel is shown in Fig. 5*D*. To generate this image, 100 junctions (B_3) were modeled as single beads whereas 150 chains (A_2) were modeled as beads connected by 10 finite-extensible nonlinear-elastic springs for each chain. Excluded volume interactions and periodic boundary conditions were enforced (46). In the simulated gel shown (Fig. 5*D*), n_λ is 0.12; primary loop chains are shown in red. In analogy to the decades-old problem for real networks, loop structures in this simulated material would be impossible to identify without labels. NDS provides such a labeling method for real materials.

Conclusions

NDS directly provides the fraction of primary loops in end-linked networks. We use NDS to quantify the primary loop fraction in PEG gels prepared via Diels–Alder end-linking. We find that loop formation defines the outcome of the gelation reaction: gels cannot form if more than 30% of network junctions contain loops. Our results show that loop formation cannot be ignored in any application, from commercial to niche, that relies on the mechanical properties of a polymer network. We anticipate that the concepts

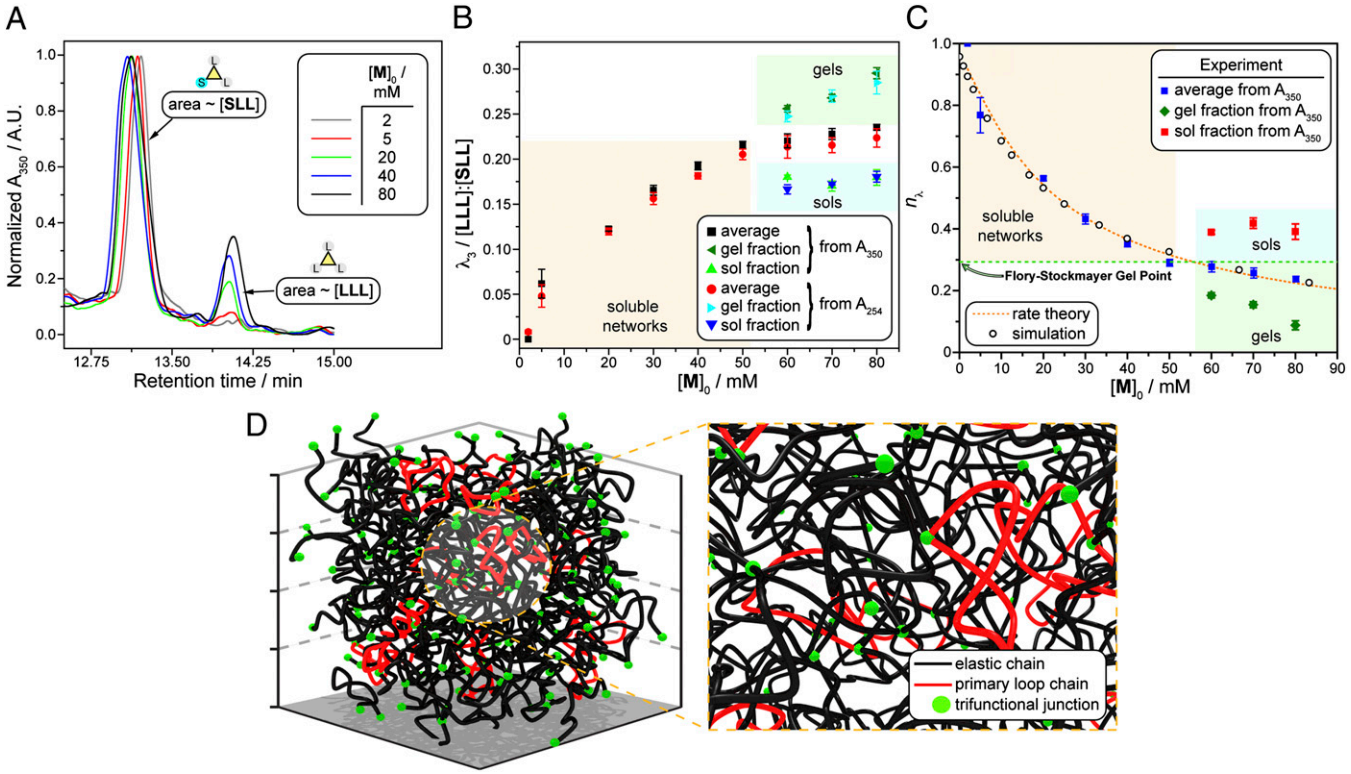

Fig. 5. Experimental and calculated loop fractions. (*A*) Normalized A_{350} network disassembly spectra for hydrolyzed networks at varied initial $[M]_0$. The concentrations of products LLL and SLL are directly proportional to the areas of the peaks at 13.9 min and 13.2 min, respectively. The amount of LLL relative to SLL decreases with increased dilution. (*B*) Plot of loop parameters, λ_3, obtained from integration of the A_{350} and A_{254} absorbance peaks corresponding to LLL and SLL. (*C*) Plot of experimental n_λ vs. $[M]_0$ along with plots obtained from two theoretical methods for predicting loop formation: Monte Carlo simulation and rate theory. (*D*) Simulated network with 12% primary loops (red).

described here will open new avenues of theoretical and experimental research related to network materials.

Materials and Methods

Procedure for Formation of Gel(O) Networks. The following procedure refers to a sample with an $[M]_0$ of 80 mM. For reactions at lower $[M]_0$ values, additional DMSO was added before mixing M and T to achieve the desired final concentration. M (4.6 mg, 4.2 μmol) was carefully weighed in a small vial. A total of 53 μL of a stock solution of T in DMSO (63 mg/mL) was added. The mixture was allowed to react at room temperature for 48 h. After this time, excess (10 equiv to 1 equiv T) of a norbornene-ethanol derivative was added to consume any potentially unreacted tetrazine groups (*SI Appendix*, Scheme S4). Ethyl vinyl ether can also be used for this quenching step. The added mass from the norbornene derivative was taken into account while searching for partially reacted junctions (observed in Fig. 4*B*). Last, excess DDQ (spatula tip) was added, and the materials were left overnight to fully oxidize.

Procedure for Gel(O) Disassembly. Gel(O) samples were swollen in fresh DMSO for 3 d. After every ~12 h, the DMSO layer was removed and fresh DMSO was added. The DMSO extracts were combined and represent the sol fraction. The gels were then broken into small pieces for easier handling. A total of 20 μL of gel(O)/DMSO mixture and 40 μL THF were transferred and mixed in an LC/MS vial. Hydrogen peroxide solution [30% (wt/wt) in H_2O, 40 μL] was added, and the mixture was vortexed for 10 s. Then, 20 μL of LiOH (2 M in water) was added, and the reaction was vortexed for 10 s. The hydrolysis was allowed to proceed for 20 min before quenching with one drop of 1 M HCl. The resulting solution was analyzed directly via LC/MS.

General Procedure for Obtaining λ_3. The integration function in Agilent ChemStation was used to automatically output the areas of each peak in the LC absorbance traces obtained from disassembled gel(O)s. The loop ratio, λ_3, was calculated from the integration ratio of the areas of SLL peak and LLL peak. Synthetic procedures, theoretical methods, and other relevant data are provided in *SI Appendix*.

ACKNOWLEDGMENTS. We thank T. A. Hatton for the use of computational resources. This work was supported by the Massachusetts Institute of Technology Department of Chemistry, Institute for Soldier Nanotechnologies US Army Research Office Contract W911NF-07-D-0004 (to B.O.), and a National Defense Science and Engineering Graduate Fellowship (to M.W.).

1. Langer R, Tirrell DA (2004) Designing materials for biology and medicine. *Nature* 428 (6982):487–492.
2. Flory PJ (1953) *Principles of Polymer Chemistry* (Cornell Univ Press, Ithaca, NY).
3. Smith BL, et al. (1999) Molecular mechanistic origin of the toughness of natural adhesives, fibres and composites. *Nature* 399:761–763.
4. Stockmayer WH, Weil LL (1945) High Polymers. *Advancing Fronts in Chemistry*, ed Twiss SB (Reinhold, New York), Vol 1, pp 61–73.
5. Stockmayer WH (1943) Theory of molecular size distribution and gel formation in branched-chain polymers. *J Chem Phys* 11:45–55.
6. Mark JE, Sullivan JL (1977) Model networks of end-linked polydimethylsiloxane chains. 1. Comparisons between experimental and theoretical values of elastic-modulus and equilibrium degree of swelling. *J Chem Phys* 66:1006–1011.
7. Stockmayer WH (1944) Theory of molecular size distribution and gel formation in branched polymers. II. General cross linking. *J Chem Phys* 12:125–131.
8. Cail JI, Stepto RFT (2007) The gel point and network formation - theory and experiment. *Polym Bull* 58:15–25.
9. Rankin SE, Kasehagen LJ, McCormick AV, Macosko CW (2000) Dynamic Monte Carlo simulation of gelation with extensive cyclization. *Macromolecules* 33: 7639–7648.
10. Stanford JL, Stepto RFT (1975) Rate theory of irreversible linear random polymerization. 1. Basic theory. *J Chem Soc Faraday Trans* 71:1292–1307.
11. Lang M, Schwenke K, Sommer JU (2012) Short cyclic structures in polymer model networks: A test of mean field approximation by Monte Carlo simulations. *Macromolecules* 45:4886–4895.
12. Wilcock DF (1947) Liquid methylpolysiloxane systems. *J Am Chem Soc* 69:477–486.
13. Lange F, et al. (2011) Connectivity and structural defects in model hydrogels: A combined proton NMR and Monte Carlo simulation study. *Macromolecules* 44: 9666–9674.

14. Lang M, Goritz D, Kreitmeier S (2005) Intramolecular reactions in randomly end-linked polymer networks and linear (co)polymerizations. *Macromolecules* 38: 2515–2523.
15. Ng LV, Thompson P, Sanchez J, Macosko CW, McCormick AV (1995) Formation of cagelike intermediates from nonrandom cyclization during acid-catalyzed sol-gel polymerization of tetraethyl orthosilicate. *Macromolecules* 28:6471–6476.
16. Stanford JL, Stepto RFT (1977) A study of intramolecular reaction and gelation during nonlinear polyurethane formation. *Br Polym J* 9:124–132.
17. Kricheldorf HR (2009) Cyclic and multicyclic polymers by three-dimensional polycondensation. *Acc Chem Res* 42(8):981–992.
18. Phadke A, et al. (2012) Rapid self-healing hydrogels. *Proc Natl Acad Sci USA* 109(12): 4383–4388.
19. Kim J, Hanna JA, Byun M, Santangelo CD, Hayward RC (2012) Designing responsive buckled surfaces by halftone gel lithography. *Science* 335(6073):1201–1205.
20. Wylie RG, et al. (2011) Spatially controlled simultaneous patterning of multiple growth factors in three-dimensional hydrogels. *Nat Mater* 10(10):799–806.
21. Kang E, et al. (2011) Digitally tunable physicochemical coding of material composition and topography in continuous microfibres. *Nat Mater* 10(11):877–883.
22. Artzi N, et al. (2011) In vivo and in vitro tracking of erosion in biodegradable materials using non-invasive fluorescence imaging. *Nat Mater* 10(9):704–709.
23. Stuart MAC, et al. (2010) Emerging applications of stimuli-responsive polymer materials. *Nat Mater* 9(2):101–113.
24. Lv S, et al. (2010) Designed biomaterials to mimic the mechanical properties of muscles. *Nature* 465(7294):69–73.
25. Davis DA, et al. (2009) Force-induced activation of covalent bonds in mechanoresponsive polymeric materials. *Nature* 459(7243):68–72.
26. Sidorenko A, Krupenkin T, Taylor A, Fratzl P, Aizenberg J (2007) Reversible switching of hydrogel-actuated nanostructures into complex micropatterns. *Science* 315(5811): 487–490.
27. Franck C, Maskarinec SA, Tirrell DA, Ravichandran G (2011) Three-dimensional traction force microscopy: A new tool for quantifying cell-matrix interactions. *PLoS ONE* 6 (3):e17833.
28. Engler AJ, Sen S, Sweeney HL, Discher DE (2006) Matrix elasticity directs stem cell lineage specification. *Cell* 126(4):677–689.
29. Lutolf MP, et al. (2003) Synthetic matrix metalloproteinase-sensitive hydrogels for the conduction of tissue regeneration: Engineering cell-invasion characteristics. *Proc Natl Acad Sci USA* 100(9):5413–5418.
30. Lutolf MP, Hubbell JA (2005) Synthetic biomaterials as instructive extracellular microenvironments for morphogenesis in tissue engineering. *Nat Biotechnol* 23(1): 47–55.
31. DeForest CA, Polizzotti BD, Anseth KS (2009) Sequential click reactions for synthesizing and patterning three-dimensional cell microenvironments. *Nat Mater* 8(8): 659–664.
32. Kloxin AM, Kasko AM, Salinas CN, Anseth KS (2009) Photodegradable hydrogels for dynamic tuning of physical and chemical properties. *Science* 324(5923):59–63.
33. Luo Y, Shoichet MS (2004) A photolabile hydrogel for guided three-dimensional cell growth and migration. *Nat Mater* 3(4):249–253.
34. Hynes RO (2009) The extracellular matrix: Not just pretty fibrils. *Science* 326(5957): 1216–1219.
35. Johnson JA, et al. (2006) Synthesis of degradable model networks via ATRP and click chemistry. *J Am Chem Soc* 128(20):6564–6565.
36. Johnson JA, Finn MG, Koberstein JT, Turro NJ (2007) Synthesis of photocleavable linear macromonomers by ATRP and star macromonomers by a tandem ATRP-click reaction: Precursors to photodegradable model networks. *Macromolecules* 40: 3589–3598.
37. Johnson JA, Baskin JM, Bertozzi CR, Koberstein JT, Turro NJ (2008) Copper-free click chemistry for the in situ crosslinking of photodegradable star polymers. *Chem Commun (Camb)* 3064–3066.
38. Kafouris D, Themistou E, Patrickios CS (2006) Synthesis and characterization of star polymers and cross-linked star polymer model networks with cores based on an asymmetric, hydrolyzable dimethacrylate cross-linker. *Chem Mater* 18:85–93.
39. Rikkou MD, Patrickios CS (2008) Well-defined networks with precisely located cleavable sites: Structure optimization and core functionality determination. *Macromolecules* 41:5957–5959.
40. Carboni RA, Lindsey RV (1959) Reactions of tetrazines with unsaturated compounds - a new synthesis of pyridazines. *J Am Chem Soc* 81:4342–4346.
41. Clavier G, Audebert P (2010) s-Tetrazines as building blocks for new functional molecules and molecular materials. *Chem Rev* 110(6):3299–3314.
42. Hansell CF, et al. (2011) Additive-free clicking for polymer functionalization and coupling by tetrazine-norbornene chemistry. *J Am Chem Soc* 133(35):13828–13831.
43. Stanford JL, Stepto RFT, Waywell DR (1975) Rate theory of irreversible linear random polymerization. 2. Application to intramolecular reaction in a-a+B-B type polymerizations. *J Chem Soc Faraday Trans* 71:1308–1326.
44. Dutton S, Stepto RFT, Taylor DJR (1996) Monte-Carlo modelling of the formation, structure and properties of polymer networks. *Angew Makromol Chem* 240:39–57.
45. Fetters LJ, Lohse DJ, Colby RH (2007) Chain dimensions and entanglement spacings. *Physical Properties of Polymers Handbook*, ed Mark JE (Springer, New York), pp 447–454.
46. Kremer K, Grest GS (1990) Dynamics of entangled linear polymer melts: a molecular-dynamics simulation. *J Chem Phys* 92:5057–5086.